Molecular Mechanisms of RNA Interference

Ross C. Wilson[2] and Jennifer A. Doudna[1,2,3,4]

[1]Howard Hughes Medical Institute, [2]Department of Molecular and Cell Biology, [3]Department of Chemistry, University of California, Berkeley, California 94720; email: doudna@berkeley.edu

[4]Physical Biosciences Division, Lawrence Berkeley National Laboratory, Berkeley, California 94720

Annu. Rev. Biophys. 2013. 42:217–39

The *Annual Review of Biophysics* is online at biophys.annualreviews.org

This article's doi: 10.1146/annurev-biophys-083012-130404

Keywords

miRNA, siRNA, RNAi, dsRNA, Argonaute, Dicer, RISC, ribonucleoproteins, crystallography

Abstract

Small RNA molecules regulate eukaryotic gene expression during development and in response to stresses including viral infection. Specialized ribonucleases and RNA-binding proteins govern the production and action of small regulatory RNAs. After initial processing in the nucleus by Drosha, precursor microRNAs (pre-miRNAs) are transported to the cytoplasm, where Dicer cleavage generates mature microRNAs (miRNAs) and short interfering RNAs (siRNAs). These double-stranded products assemble with Argonaute proteins such that one strand is preferentially selected and used to guide sequence-specific silencing of complementary target mRNAs by endonucleolytic cleavage or translational repression. Molecular structures of Dicer and Argonaute proteins, and of RNA-bound complexes, have offered exciting insights into the mechanisms operating at the heart of RNA-silencing pathways.

Contents

A BIOLOGICAL VIEW OF RNA INTERFERENCE 218
Small Regulatory RNAs in Cellular Function and Dysfunction 218
Biogenesis and Action of miRNA and siRNA 219
ACTIVITY, STRUCTURE, AND INTERACTIONS OF miRNA PATHWAY PROTEINS 221
Microprocessor 221
Dicer 223
dsRBPs 226
Argonaute 228
GW-PABP Interface 232
C3PO 233
FRONTIERS IN RNAi BIOPHYSICS 233
Strand Selection 233
P Bodies 234
Kinetics of Repression, Decay, and RISC Turnover 234

A BIOLOGICAL VIEW OF RNA INTERFERENCE

Small Regulatory RNAs in Cellular Function and Dysfunction

The discovery of RNA interference (RNAi) revolutionized our understanding of gene regulation by revealing an array of related pathways in which small, ~20- to 30-nucleotide (nt) noncoding RNAs and their associated proteins control the expression of genetic information (7). In processes that are widespread in plants and animals (80), each small RNA associates with an Argonaute family protein to form a sequence-specific, gene-silencing ribonucleoprotein with specificity conferred by base-pairing between the small (guide) RNA and its target mRNA.

RNAi was initially discovered in the form of a single microRNA (miRNA) in the *Caenorhabditis elegans* genome (48). Eventually such miRNAs were found to be widespread: As much as 5% of the human genome is dedicated to encoding and producing the >1,000 miRNAs that regulate at least 30% of our genes (38, 58). RNAi is charged with controlling vital processes such as cell growth, tissue differentiation, heterochromatin formation, and cell proliferation. Accordingly, RNAi dysfunction is linked to cardiovascular disease, neurological disorders, and many types of cancer (53). RNAi pathways transcend mere expansion of the gene regulation toolkit: They confer a qualitative change in the way cellular networks are managed. This prompts consideration of the fascinating possibility that we owe our sentience to small RNAs, as the number of miRNAs present in a genome appears to correlate with the complexity of the organism (3).

In contrast to miRNA, short interfering RNA (siRNA) typically describes exogenous synthetic or viral inducers of RNAi. Such small RNAs have been used in biomedical research to great effect, allowing selective repression of genes of interest. Furthermore, immense effort has been exerted in hopes of developing siRNA-based therapies to combat genetic or viral disease. Although the field shows great promise, challenges with delivery as well as harmful off-target effects have prevented any such drug from reaching the market so far (14). In parallel with this effort, advances in mechanistic understanding of these pathways have been impressive, providing increasing insights into the molecular structures and activities responsible for small RNA–mediated genetic control.

nt: nucleotide(s)

Argonaute: a protein capable of binding short ssRNAs and, in some cases, cleaving a bound complementary strand

Such insights will be essential to future success in harnessing RNAi and related processes for both therapeutics and genome engineering.

This review focuses primarily on structural and mechanistic studies of the human miRNA pathway. In many cases, macromolecular structures and interactions that are part of miRNA pathways are analogous to those responsible for siRNA activities. In contrast, the key molecular players involved in the germ line–specific PIWI-interacting RNA (piRNA) pathway have remained so mysterious that little biophysical study has been possible until very recently. Emerging structures of the endoribonuclease Zucchini provide a foundation for mechanistic study of piRNA biogenesis (35, 66, 91).

Biogenesis and Action of miRNA and siRNA

The three pathways of RNAi (miRNA, siRNA, piRNA) share a common mode of action: The minimal effector is a ribonucleoprotein complex comprising an Argonaute family protein bound to a single-stranded ~20- to 30-nt RNA that grants specificity via base-pairing interactions with the gene target. In miRNA and siRNA pathways, this is known as the RNA-induced silencing complex (RISC) and it drives silencing of a target mRNA via degradation and/or transcriptional repression (**Figure 1**). The cellular origins of miRNA and siRNA are somewhat disparate: miRNAs are derived from the genome, whereas siRNAs may be endogenous or arise via viral infection or other exogenous sources (7). Another key difference occurs in the double-stranded RNA (dsRNA) precursors of each: siRNA duplexes feature perfect base-pairing, whereas miRNA helices contain mismatches and more extended terminal loops. Despite their differing origins, these processing pathways converge once either type of RNA assembles into the RISC.

Typically, the genesis of a miRNA occurs in the nucleus with a transcript known as a primary miRNA (pri-miRNA); such transcripts are at least 1,000 nt long, containing single or clustered double-stranded hairpins that bear single-stranded 5′- and 3′-terminal overhangs and ~10-nt distal loops (75). A pri-miRNA is cropped by the microprocessor complex, comprising Drosha, an RNase III family enzyme, and DiGeorge syndrome critical region gene 8 (DGCR8), a protein containing two double-stranded RNA-binding domains (dsRBDs) (42). DGCR8 recognizes the pri-miRNA's junction of stem and single-stranded RNA, which likely helps position Drosha for the endonucleolytic cleavage it performs on the stem ~11 base pairs (bp) from the junction (31). The resulting ~65- to 70-nt precursor miRNA (pre-miRNA) associates with transport facilitators Exportin-5 and RanGTP and is exported to the cytoplasm (54).

In the cytoplasm, the processing pathways converge for endogenous miRNAs and for typically exogenous siRNAs. Both types of RNAi precursors are trimmed down to a dsRNA duplex of the appropriate size for loading onto an Argonaute protein; this is typically performed by a Dicer enzyme. Dicers are large endoribonucleases containing a helicase domain and an internally dimerized pair of RNase III domains, but this composition can vary between organisms (80). Before or after they are excised, introns may serve as viable substrates for microprocessor or Dicer, acting as pri- or pre-miRNAs, respectively (42). In plants, dicing precedes methylation of the 3′-terminal nucleotide's 2′-hydroxyl by the methyltransferase HEN1 (34). The resulting dsRNA is a duplex of 21- to 25-nt strands, bearing a 2-nt overhang at each 3′ terminus and a phosphate group at each recessed 5′ terminus (78). With this enzymatic step and the subsequent loading of duplex onto Argonaute, Dicer may be aided by a dsRNA-binding protein (dsRBP) such as TAR RNA-binding protein (TRBP). These three proteins (Dicer, Argonaute, and a dsRBP) constitute a minimal RISC-loading complex (RLC), which is responsible for generating diced dsRNA and loading it onto Argonaute (61). Once the dsRNA helix is presented to Argonaute, the 3′ terminus and 5′ phosphate of the guide strand are bound by the protein's PAZ (named for its presence

RNA-induced silencing complex (RISC): the minimal RNA-induced silencing complex contains an Argonaute protein bound to a guide strand; the effector of silencing

Microprocessor: the nuclear protein complex of Drosha and DGCR8; responsible for cleavage of pri-miRNAs into pre-miRNAs

dsRBD: double-stranded RNA-binding domain

Dicer: an endoribonuclease responsible for cleaving long dsRNAs and/or pre-miRNAs to dsRNA duplexes of a specific length

dsRBP: double-stranded RNA-binding protein

RISC-loading complex (RLC): a complex composed of at least Argonaute, Dicer, and a dsRBP such as TRBP; responsible for generating diced dsRNA and loading it onto Argonaute

TRBP: TAR RNA-binding protein

Guide strand: ssRNA of ~20–30 nt that base-pairs with complementary targets, thus providing the specificity of silencing processes

in PIWI, Argonaute, and Zwille proteins) and MID domains, respectively, generating the RISC. RISC loading is coincident with the strand selection step, wherein one strand of the duplex is bound to Argonaute to direct silencing and the other strand is discarded. These strands are known as the guide and passenger strands, respectively, and their selection is a key determinant of the silencing that follows. The transient complex consisting of Argonaute bound to the guide strand and a passenger strand that has yet to be cleaved and/or dissociate is known as the pre-RISC. In the case of the miRNA pathway, the strand from the duplex that is most commonly loaded is known as the miRNA and the opposing strand is termed the miRNA*.

ssRNA: single-stranded RNA

The RISC performs cellular surveillance, binding single-stranded RNA (ssRNA) such as mRNA with complementarity to the Argonaute-bound guide strand. Guide strand nucleotides

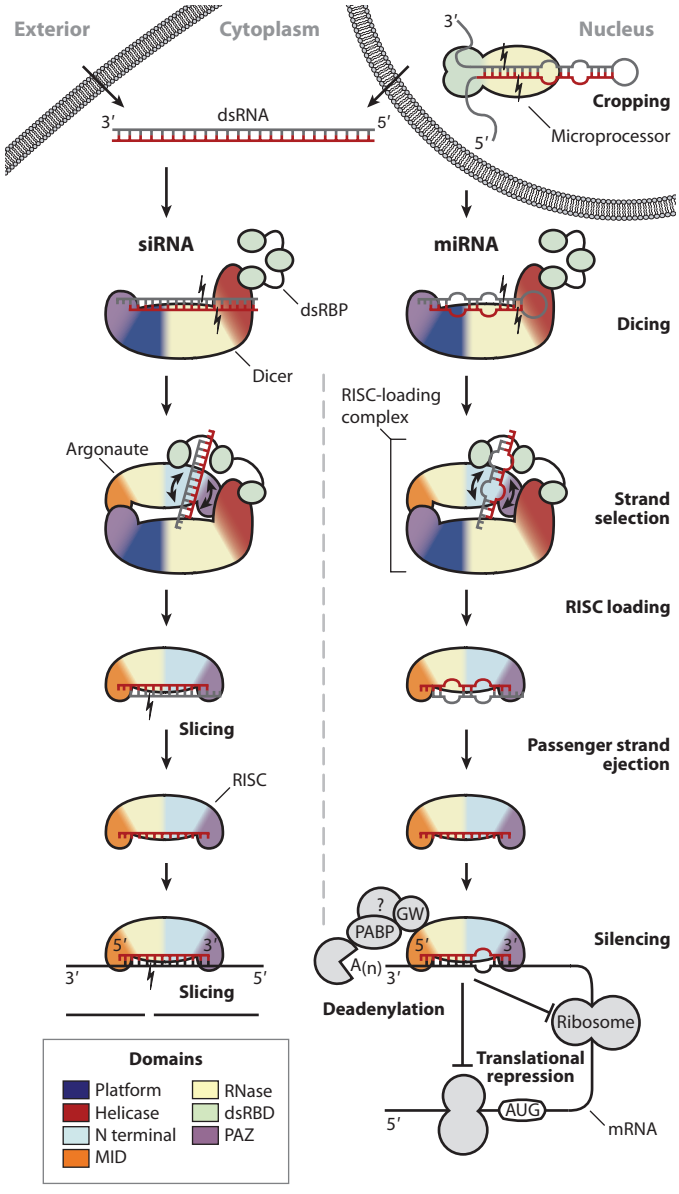

2–6 constitute the seed sequence and initialize binding to the target. This binding need not involve perfect complementarity, and the extent of base-pairing influences how the subsequent silencing transpires. In cases of perfect complementarity, target cleavage can occur if the Argonaute present bears catalytic activity (as is true for just one of the four human AGO proteins, Ago2). The RISC can also induce nonendonucleolytic translational repression before or after initiation; this may be followed by deadenylation and degradation. Additional cellular machinery is responsible for the processes downstream of target binding, and the Argonaute-binding protein GW182 is a key mediator in recruiting these additional components to the RISC and in localizing silencing activity to cytoplasmic loci known as processing (P) bodies (20). These complicated gene-silencing mechanisms were initially unclear and appeared daunting, but a recent surge of information has shed light on major pathways and is reviewed in Reference 22.

Seed sequence: positions 2–8 of the guide stand; a region whose target complementarity is critical in determining the efficacy of silencing

aa: amino acid

ACTIVITY, STRUCTURE, AND INTERACTIONS OF miRNA PATHWAY PROTEINS

Microprocessor

Before their export to the cytoplasm for further processing and silencing, nuclear pri-miRNAs must be recognized and cleaved. These respective tasks are carried out by the proteins Drosha and DGCR8 (known as Pasha in invertebrates), which together constitute the microprocessor complex. As with Dicer, Drosha proteins belong to the RNase III family, whose members contain a dimeric active site (60). The minimal endonucleolytic active site is composed of two ~100-amino-acid (aa) RNase III domains; in bacterial or yeast (class 1) enzymes, these domains result from homodimerization of two identical protomers. In contrast, the pair of RNase III domains composing the active sites of Drosha (class 2) and Dicer (class 3) enzymes are provided as an adjacent pair on the same chain, forming a pseudodimer. Regardless of a given protein's class, the most C-terminal RNase III domain is followed by a ~70-aa dsRBD, which confers sequence-nonspecific dsRNA binding. All three classes of RNase III enzymes utilize each catalytic domain to cleave a single strand of the dsRNA substrate, working in unison to produce new dsRNA termini bearing 2-nt 3′-terminal overhangs and 5′-terminal phosphate groups (60).

In the context of the microprocessor complex, Drosha performs cleavage consistent with its identity as an RNase III enzyme (49). The portion of the protein N-terminal to its paired catalytic domains is typical of a class 2 RNase III in that it contains a proline-rich region, but the function

Figure 1

The siRNA (*left*) and miRNA (*right*) pathways of RNA interference. Protein domain architecture is approximated in the illustrations here, and domain coloring is maintained in subsequent figures. For clarity, one dsRBD has been omitted from each of the Dicer and microprocessor illustrations. The siRNA pathway (*left*) begins with Dicer's cleavage of dsRNA of exogenous or nuclear origin. The resulting siRNA duplex is loaded onto Argonaute by the RISC-loading complex, which comprises Dicer, a dsRBP protein such as TRBP, and an Argonaute protein. The passenger strand (*gray*) is cleaved and ejected. The guide strand (*red*) remains bound to Argonaute, forming the RISC. The RISC binds to complementary target sequences (*black*) and silences them via the slicing activity of Argonaute. In the miRNA pathway (*right*), a primary miRNA transcript is cropped by the microprocessor complex, which consists of the endonuclease Drosha bound to DGCR8. The resulting pre-miRNA is exported to the cytoplasm, where dicing and RISC loading take place as in the siRNA pathway. Passenger strand (*gray*) ejection may take place without concomitant cleavage, and the guide strand (*red*) drives silencing as part of the mature RISC. In cases of a catalytically inactive Argonaute or partial complementarity to the target (*black*), silencing takes place via pre- or post-initiation translational repression and deadenylation followed by degradation of the mRNA.

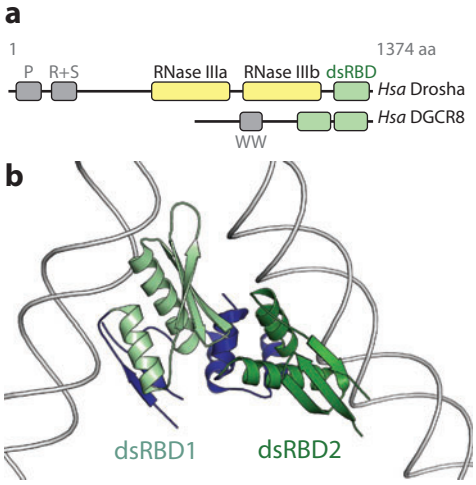

Figure 2

The microprocessor complex. (*a*) Domain structures of the human microprocessor constituents Drosha and DGCR8. Regions rich in proline (P), arginine and serine (R+S), or tryptophan (W) are labeled. (*b*) The crystal structure of the DGCR8 core (PDB ID: 2YT4). Models of dsRNA are oriented on the basis of typical dsRBD binding and show that the DGCR8 core cannot use both dsRBDs to bind a single pre-miRNA unless extensive deformation of the helix occurs.

of this portion remains unknown (**Figure 2*a***). Drosha's C-terminal dsRBD is canonical in its sequence and tertiary structure (64) and is required for pri-miRNA processing in vivo (2) but does not appear to play a substantial role in substrate binding or recognition in vitro (101), tasks instead performed by DGCR8 (31). Accordingly, Drosha cleaves pri-miRNAs indiscriminately in the absence of DGCR8 (27). DGCR8's dsRNA binding is carried out by a pair of dsRBDs in its C-terminal half; its N terminus contains a structurally characterized, heme-binding dimerization domain (79) and is otherwise of unknown structure and function, though its tryptophan-rich region has been hypothesized to interact with the proline-rich region of Drosha's N terminus (27) (**Figure 2*a***).

The structure of the DGCR8 core. The crystal structure of DGCR8's dsRBD pair revealed two domains, each adopting the traditional fold: an α/β sandwich with the terminal α-helices resting atop a three-stranded β-sheet (**Figure 2*b***). These two domains are surrounded by several additional secondary structural elements that contribute to a well-ordered quaternary structure (the DGCR8 core), orienting the two dsRBDs with respect to each other without disrupting either individual structure from the canonical geometry. The DGCR8 domains were crystallized in the absence of RNA, yet concomitant binding studies via electrophoretic mobility shift assay (EMSA) and fluorescence resonance energy transfer (FRET) revealed that the dsRBDs interact with dsRNA but not with ssRNA. Although the dsRNA affinity is anticipated for a pair of orthodox dsRBDs, the lack of affinity for ssRNA is somewhat surprising because the DGCR8-binding site is a junction between a helical stem and two flanking strands of ssRNA (stem-ssRNA junction) (**Figure 1**). This binding site is inferred on the basis of cleavage assays that reveal DGCR8 to be the factor responsible for correctly positioning and orienting the microprocessor for Drosha-catalyzed cleavage ~11 bp from the stem-ssRNA junction (31), but it remains unclear which region of DGCR8 or Drosha is responsible for recognition of the flanking ssRNA.

Without detectable affinity for ssRNA, it is unknown how DGCR8 is so reliably positioned at the stem-ssRNA junction instead of binding promiscuously along the pri-miRNA stem. Curiously, the only reported evidence for ssRNA-specific binding by any microprocessor component implicates the serine/arginine-rich region of Drosha's N terminus (102), though this probably explains the microprocessor's preference for a distal ~10-nt loop on the pri-miRNA substrate rather than addresses DGCR8's positioning at the stem-ssRNA junction.

Higher-order assemblies between the microprocessor and pri-miRNA. Efforts are under way to model the active state of the microprocessor complex interacting with its pri-miRNA substrates. The two dsRBDs of the DGCR8 core offer their RNA-binding surfaces such that they cannot simultaneously bind a pri-miRNA without a major distortion from A-form geometry (**Figure 2*b***); FRET-based evidence for such bending has been reported, but the possibility remains that the DGCR8 core's two domains bind to separate pri-miRNAs (81). Evidence for such multimeric assembly is provided by an electron tomography study of the association between DGCR8 and a pri-miRNA, which revealed a ~370-kDa particle consistent with a single pri-miRNA bound to six DGCR8 protomers or four pri-miRNA:DGCR8 heterodimers, among other configurations (23). Such larger assemblies might be expected because many miRNAs originate from pri-miRNAs clustered on a single transcript.

Recent cellular imaging studies have precisely tracked the nuclear localization of Drosha and DGCR8 over time, revealing that they colocalize simultaneously on unspliced, intronic pri-miRNA and that Drosha tends to dissociate after cleavage, whereas DGCR8 is likely to remain bound to the processed pre-miRNAs before their nuclear export (2). The former finding builds on an earlier report that the microprocessor associates with the spliceosome, providing mounting evidence that cropping takes place before splicing is complete (40).

Dicer

The Dicer family of class 3 RNase III enzymes is vital to siRNA and miRNA pathways. These proteins generate dsRNAs suitable for loading onto an Argonaute protein, a process in which Dicer may participate as part of the RLC. Dicer's active center is derived from bacterial class 1 RNase III enzymes, which comprise an RNase III domain with a C-terminal dsRBD (80). Bacterial enzymes dimerize to achieve concerted cleavage of both strands of a dsRNA substrate. Class 3 Dicer enzymes accomplish similar dsRNA cleavage using a pseudodimer of RNase III domains on a single polypeptide with a single C-terminal dsRBD (60). N-terminal to these paired active sites is a PAZ domain, which recognizes the dsRNA end characteristic of RNAi intermediates (57) (**Figure 3*a***). The PAZ and RNase III domains act together as a molecular ruler to mete out diced strands of RNA appropriate for a given organism's silencing machinery, as discussed in greater depth below.

A distinguishing characteristic of Dicer is the superfamily 2 helicase domain often found at its N terminus. This ≥600-aa domain belongs to the eukaryotic RIG-I family of helicases, which is characterized by a bilobal architecture comprising DExD/H and helicase C regions, the former of which is expected to bind and potentially hydrolyze ATP (104). The function of this helicase domain is still being defined in the case of humans, whereas the helicase domain can recognize either miRNA or siRNA precursors (see below) in the Dicer enzymes of *Drosophila*. In some cases Dicer's helicase domain also contains a binding site for a dsRBP such as TRBP in humans.

Dicer's domain structure varies between organisms, yet its principal dicing function is preserved. *Giardia intestinalis* Dicer lacks a helicase domain (59), and the budding yeast *Kluyveromyces polysporus* equivalent is further pared down, lacking a PAZ domain and bearing an RNase III

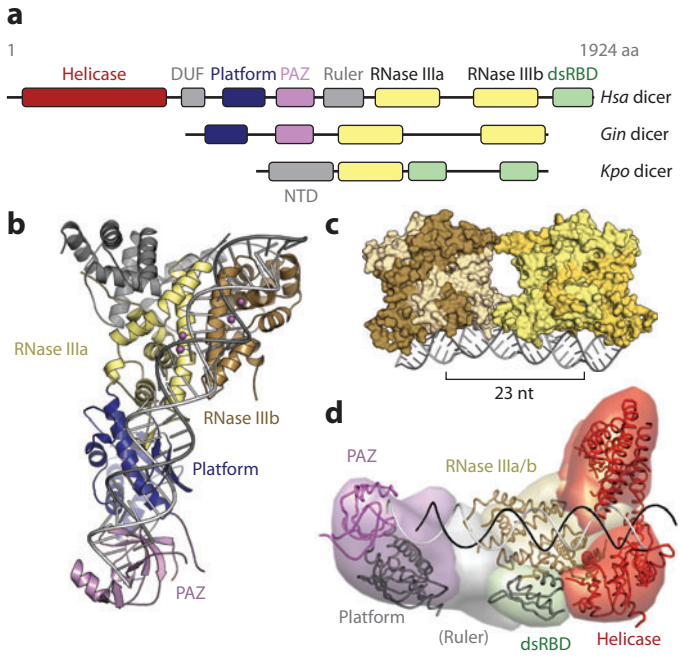

Figure 3

The diverse architecture of the Dicer family. (*a*) Domain structures of Dicer enzymes from humans (*Hsa*), *Giardia intestinalis* (*Gin*), and *Kluyveromyces polysporus* (*Kpo*). The domain of unknown function (DUF) and the anticipated ruler domain are indicated for the human enzyme. *K. polysporus* Dicer bears a single RNase III domain and an N-terminal domain (NTD) that mediates dimerization. (*b*) Dicer's measurement and cleavage of pre-miRNA as illustrated by the *G. intestinalis* crystal structure (PDB ID: 2FFL). Purple spheres represent erbium atoms present in the crystal, which reflect the position of the Mg^{2+} ions critical to RNase III enzyme catalysis. In this model, the 2-nt 3′-terminal overhang of a dsRNA substrate is docked onto Dicer's PAZ domain, orienting it for two cleavage events in the active site 65 Å away, generating a 25-nt duplex. (*c*) The inside-out mechanism of *K. polysporus* Dicer (PDB ID: 3RV0). This enzyme lacks a PAZ domain and uses neighboring molecules to measure its product. This model depicts two homodimers of the enzyme, each bearing a single RNase III domain, contacting each other to measure a 23-nt product. The resulting dsRNA originates from the center of the substrate duplex, in contrast to the end-derived products generated by PAZ-containing Dicers. (*d*) The global architecture of human Dicer. Homologous domains of known structure have been docked onto a segmented electron microscopic map (PDB IDs: 4A36, 2KOU, 2FFL, and 3C4T). The helicase domain resembles a clamp and is optimally oriented to guide an incoming dsRNA substrate (*black and white coil*) toward the RNase IIIa/b active center and PAZ domain. Relative to the *G. intestinalis* enzyme, a ruler domain is inserted and the PAZ domain is reoriented with respect to the RNase III catalytic center. These changes likely relate to the fact that human Dicer products are four nucleotides shorter than those of *G. intestinalis*.

domain (96) (**Figure 3*a***). These helicase-lacking enzymes may have lost dsRBP binding capability as well, considering the aforementioned interface. In a case of specialization, *Drosophila* employs a pair of Dicer enzymes and corresponding dsRBPs to create parallel processing pathways for siRNAs and miRNAs (9). Plants such as *Arabidopsis thaliana* take such specialization further with four Dicer-like proteins (DCL1–4): DCL1 for generation of 21-nt miRNAs and DCL2–4 for processing of siRNAs of 22, 24, or 21 nt, respectively (74).

Dicing activity. Dicer's principal function is to recognize dsRNA precursors from the RNAi pathway and sever both strands to generate dsRNAs of a specific length, typically 21–25 nt (4). Recognition and cleavage of a generic segment of dsRNA helix can be expected of any enzyme

system bearing a pair of RNase III domains. These dimerized domains bear two active sites and a flat, positively charged surface that can accommodate a long RNA helix. Each active site bears four acidic residues that coordinate two Mg^{2+} ions used in phosphodiester hydrolysis of each RNA strand (26, 84) (**Figure 3*b***). The dsRNA terminus characteristic of RNAi pathway precursors (a 2-nt overhang on the 3′ terminus and a phosphate-bearing 5′ terminus) can be recognized by the Dicer's PAZ domain, as was revealed by a crystal structure of human Argonaute's similar PAZ domain bound to one such RNA terminus (see below) (57).

The RNA-measuring component of Dicer's function was revealed upon structure determination of the *G. intestinalis* version of the protein, wherein the PAZ domain is located 65 Å from the catalytic center (59) (**Figure 3*b***). This distance corresponds to the length spanned by ∼25 bp of dsRNA, which is consistent with the 25- to 27-nt products generated by *G. intestinalis* Dicer. The distance between the end-binding PAZ domain and the RNase III cleavage sites is determined by structural orientation of the domains; these domains likely undergo rearrangement in other Dicer incarnations to produce the observed products of differing lengths. *G. intestinalis* Dicer lacks the typical N-terminal helicase and C-terminal dsRBD domains, suggesting that these elements fulfill roles supplementary to dicing (59). This finding is consistent with the observation that a truncated form of human Dicer lacking helicase and dsRBD domains retained dicing activity (55). More recent studies show that the dsRBD can rescue activity in a form of human Dicer lacking its PAZ domain, though the resulting products vary in length as might be expected (56).

Also lacking a helicase domain is Dicer of the budding yeast *K. polysporus*, Dcr1, which represents an extremely pared down version of the enzyme that nevertheless retains its ability to specify product size in the absence of a PAZ domain (**Figure 3*a***). Its single RNase III domain dimerizes to cleave dsRNA; despite this similarity to class 1 bacterial enzymes, *K. polysporus* Dcr1 remains classified with other class 3 enzymes owing to similarity in sequence and active site composition. A crystal structure and concomitant mechanistic studies revealed that Dcr1 dimers cleave dsRNA at precise intervals by abutting each other along the helix and measuring the product based on the distance (23 nt) occupied by the protein structure between the neighboring pairs of active sites (96) (**Figure 3*c***). This mechanism contrasts starkly to that of canonical Dicers, which measure from a dsRNA's terminus; *K. polysporus* Dcr1 begins at an arbitrary point within a dsRNA and works outward in 23-nt steps. Its mode of action is predicated on slow substrate release, which was indeed reported and is likely facilitated by one or both of the enzyme's two C-terminal dsRBDs (96).

The role of Dicer's helicase domain in RNA recognition. The function of Dicer's helicase domain is best understood in the case of *Drosophila* Dicer-2. Dicer-2 is specialized to process siRNA precursors, which are longer, perfectly paired dsRNAs; Dicer-1 handles the shorter and imperfect pre-miRNA hairpins (9). The canonical helicase domain of Dicer-2 consumes ATP to translocate the enzyme with respect to a long dsRNA, enabling processive generation of many siRNA duplexes from a single substrate helix (9). Furthermore, this domain facilitates processing of dsRNA substrates that lack the characteristic 2-nt 3′-terminal overhang (97). The divergent Dicer-1 helicase domain contains a helicase C moiety but lacks the DExH/D lobe, providing an explanation for its inability to translocate along dsRNA. This modification does not completely abolish RNA binding: The domain has been implicated in recognition of the ssRNA loops characteristic of pre-miRNA hairpins, thus contributing to the enzyme's specificity (90).

The parallel processing pathways for siRNA and miRNA are mirrored by a duplication of RNAi machinery in *Drosophila*, leading to differing, specialized helicase domains. But in humans, a single Dicer is responsible for handling both types of precursors. How does the single human Dicer recognize and process both types of substrates? Has the human helicase domain evolved greater adaptability in substrate specificity or has it experienced a partial loss of function? These

questions remain to be fully resolved, but it seems that a loss of function has taken place since the human domain appears better adapted for the miRNA pathway. Unlike for *Drosophila* Dicer-2, RNA processing for human Dicer is ATP independent; thus, the helicase domain is unlikely to be involved in translocation of long dsRNA (103). Two biochemical reports implicate it in aiding miRNA processing, probably via binding of the pre-miRNA loop (56, 82).

A recent electron microscopic (EM) study elegantly employed extensive tagging and deletion of domains to deduce for the first time the global domain orientation of human Dicer (46) (**Figure 3*d***). One surprising observation was the reorientation of the RNase III nuclease core with respect to the PAZ domain when comparing the structure of human Dicer to that of *G. intestinalis* Dicer (59). This global reorganization likely stems from the 4-nt (one-third of a dsRNA helical turn) length difference between the products of the two enzymes and the differing associated geometric requirements for cleavage (46). Similar rearrangements might be expected in Dicers producing products with other lengths. Data interpretation was bolstered by structure determination of the helicase RIG-I, which provided a model that was readily positioned into the EM density for the related helicase domain of human Dicer (43). The EM reconstruction of the elongated human Dicer revealed a helicase that is distal from the PAZ domain, with the paired RNase III active sites resting in between. This architecture is consistent with both known functions of the helicase domain. For pre-miRNAs, the PAZ domain recognizes the 2-nt overhang and the helicase recognizes the hairpin's loop on the other end. For long dsRNA substrates, the helicase domain can feed the helix toward the catalytic center to generate multiple siRNAs. Accordingly, a concomitant EM reconstruction of the siRNA-specific *Drosophila* Dicer-2 revealed an architecture remarkably similar to that of human Dicer (46).

Dicer's interactions with other proteins. As part of the RLC, Dicer associates with an Argonaute protein and a dsRBP such as TRBP in humans. The mechanistic implications of these interactions for the processes of strand selection and RISC loading are discussed below. The dsRBPs of RNAi tend to comprise three dsRBDs connected by long, flexible linkers. The third such domain of TRBP interacts with a region of Dicer's helicase located between the DExD/H and helicase C lobes (13). The interaction with Argonaute takes place between a portion of that protein's PIWI domain and a region within the RNase III domain closer to the N terminus of Dicer (76, 85). The conserved Argonaute-interacting site on Dicer is present only in vertebrates, so Argonaute binding must be absent or manifested differently in other nonvertebrate RNAi systems (76).

A solution structure of the DUF283 domain of *A. thaliana* DCL4 revealed a noncanonical dsRBD fold that interacts with the second dsRBD of DRB4, a dsRBP homolog of TRBP (74). DRB4 contains two dsRBDs but lacks a predicted third C-terminal dsRBD typically found in dsRBPs of RNAi pathways. This third dsRBD is commonly implicated in interactions with Dicer's helicase, so *A. thaliana* appears to have evolved a different strategy for recognition between the two proteins. Indeed, the paralogous *Arabidopsis* protein pair DCL1 and DRB1 (also known as HYL1) similarly interact via their respective DUF283 and second dsRBP domains (74).

dsRBPs

Dicing and RISC loading are aided to varying degrees by dsRBPs, which associate with a Dicer protein and typically comprise two or three dsRBDs. The dsRBD is widespread and typically recognizes dsRNA on the basis of its A-form helical shape with moderate to high affinity and in a sequence-nonspecific manner (17). These proteins typically contain a C-terminal noncanonical dsRBD dedicated to protein interaction instead of dsRNA binding. TRBP is the best characterized dsRBP of the human pathway, and its 366-aa polypeptide bears three ~70-aa dsRNA-binding

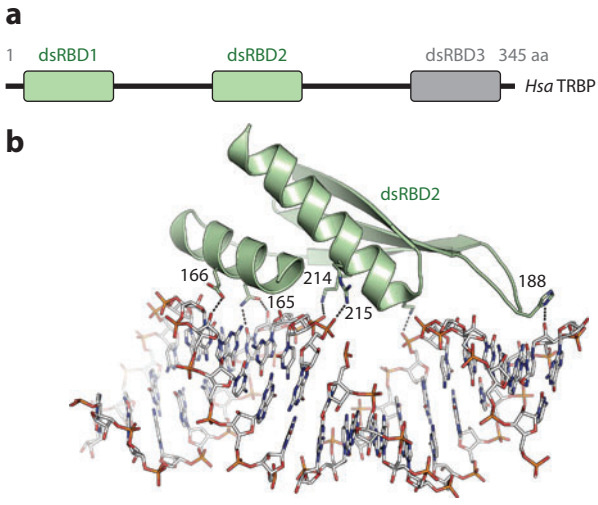

Figure 4

The structure of dsRNA-binding proteins. (*a*) The domain structure of human TRBP, a typical dsRBP of the RNAi pathway. The well-folded dsRBDs are separated by flexible ~70-aa linkers, lending the protein a beads-on-a-string quality. The first two domains bind dsRNA and the third instead binds to Dicer. (*b*) The crystal structure of the second dsRBD of TRBP in complex with dsRNA (PDB ID: 3ADL). The protein uses three interfaces to recognize successive portions of minor, major, and minor groove along one face of a helix.

domains separated by two ~70-aa stretches of disordered linker (**Figure 4*a***). Resembling beads on a string, this domain architecture suggests that the protein may be involved in a dsRNA handoff between Dicer and Argonaute (92), but detailed mechanistic evidence is scarce. RNAi pathway dsRBPs have been implicated in strand selection (8), stabilization of the miRNA-generating complex (72), tuning of mature miRNA length (25, 47), and segregation of siRNAs into distinct pathways (32, 68).

Functional coupling between Dicers and dsRBPs. The multiplicity and diversity of dsRBPs impede facile prediction of their roles in RNAi pathways. *A. thaliana* represents an extreme case, bearing five dsRBPs serially named DRB1–5. Although these might be expected to generally pair off with the four Dicer-like proteins DCL1–4, such pairings are observed only for DRB1/DCL1, which produces miRNAs, and for DRB4/DCL4, which processes siRNAs (12). DRB2, DRB3, and DRB5 seem somewhat redundant, whereas DCL2 and DCL3 appear to function unhindered in the absence of a dsRBP partner (12). *Drosophila* harbors a slightly more streamlined system in which Dicer-1 pairs with the PB isoform of dsRBP Loquacious (Loqs-PB) to process pre-miRNAs and Dicer-2 binds either R2D2 or Loqs-PD to process siRNAs of exogenous or endogenous origin, respectively (32).

The human system includes a solitary Dicer and two dsRBPs, TRBP and PACT, that play poorly delineated roles in small RNA processing (50). Although it is tempting to speculate that one human dsRBP is responsible for siRNA while the other tends to miRNA, such evidence has yet to be found. Human Dicer's interaction with both TRBP and PACT is complicated because each of the two dsRBPs has been reported to homodimerize and to form heterodimers with the other (45). These dimerization interactions have been localized to the atypical yet conserved C-terminal dsRBD of each protein, which also recognizes Dicer (13). Until it is determined whether any of these binding interfaces are mutually exclusive, there are at least two plausible scenarios: Dicer can

bind to TRBP or PACT interchangeably, or Dicer can bind to TRBP and PACT simultaneously at distinct sites.

Structure and RNA recognition of dsRBPs. Structural study of dsRBPs has been fruitful, although not particularly illuminating regarding mechanism. Structures have been reported for the first two dsRBDs from TRBP, dsRBD1 and dsRBD2, with the latter bound to dsRNA (98). The RNA-bound structure adopts an α/β sandwich that embodies the binding mode characteristic of a canonical dsRBP: The A-form helical geometry of dsRNA is recognized using protein loops and helices to bind the phosphate backbone at three points: two regions of minor groove surrounding a major groove along one face of the helix (17) (**Figure 4*b***). RNA recognition is shape based and not sequence specific, as might be expected in consideration of the requirements of the system. The implications of this mode of recognition for strand selection are discussed below. Protein sequence differences subtly tune the dissociation constants of isolated dsRBD1 and dsRBD2 to 220 and 113 nM, respectively, and their collaborative affinity is 0.24 nM in the context of the full-length protein (98). Similar variability in affinity is likely to be found on other RNAi pathway dsRBDs with little or no deviation from the canonical fold. No structural information is available for the noncanonical RNAi dsRBDs, which employ unknown means to recognize Dicer and/or other noncanonical dsRBDs.

Argonaute

The functional lynchpin of all RNAi pathways is an Argonaute family protein bound to a strand of silencing RNA, which forms the minimal effector complex known as the RISC. The RISC performs cellular surveillance, silencing ssRNA sequences complementary to its bound guide strand. Argonaute proteins are found in bacteria, archaea, and eukaryotes. Whereas the former two groups contain Argonautes of poorly defined function (80), their eukaryotic counterparts have evolved into two clades with distinct functions. Proteins of the AGO clade mediate cytosolic gene silencing while bound to siRNAs or miRNAs, and PIWI clade proteins interact with piRNAs to manage mobile genetic elements of the germ line (29). Humans have four proteins of the former clade, Ago1–4. Of these four, only Ago2 exhibits slicer activity: the endonucleolytic cleavage of bound target ssRNA (37). Such activity is not required for gene silencing; human AGO proteins can accomplish regulation by binding a target, repressing its translation, and recruiting cellular machinery to induce deadenylation and mRNA decay (36).

The key functions of Argonaute are recognition of guide strand termini, target cleavage, and recruitment of other proteins involved in silencing. Eukaryotic Argonaute proteins adopt a bilobal architecture, with each lobe containing either the N-terminal (or simply N) and PAZ domains or the MID and PIWI domains (**Figure 5*a*,*b***). A series of illuminating crystal structures has provided the initial details of how individual domains function in isolation, ultimately clarifying how they work together in the context of a competent RISC complete with guide strand and target ssRNA. Via their similarity, structures of ternary complexes between RISC and target have shed light on the approximate structure of the pre-RISC awaiting passenger strand dissociation.

Recognition of guide strand termini by Argonaute. The first Argonaute fragment structures revealed that the PAZ domain is responsible for recognizing 2-nt 3′-terminal overhangs, a finding with functional implications for PAZ-containing Dicer enzymes as well. The domain provides a pocket to accommodate 2 nt of a 3′ terminus while making less extensive contacts with the 5′ terminus present in many dsRNAs of RNAi pathways (52, 57, 99) (**Figure 5*c***). Side chains of the PAZ domain partake in extensive polar interactions with the bound RNA's buried phosphate

group and sugar hydroxyls, though there are no specific contacts to the bound 2′-OH groups, consistent with RNAi being tolerant of such modifications (11, 57). The terminal nucleobase is partially buried in a hydrophobic cavity and the edges of the terminal two bases remain exposed to solvent, indicative of sequence-nonspecific recognition (57).

In contrast to the indiscriminate 3′-terminal binding, 5′ termini tend to bear a particular nucleotide depending on the identity of the associated Argonaute protein (41). Crystal structures of eukaryotic Argonaute MID domains, some in complex with the four different nucleoside monophosphates mimicking the 5′ end of miRNAs, revealed specific contacts between a rigid loop in the MID domain and the nucleobase of UMP or AMP (5, 24) (**Figure 5*d***). The electrostatic environment generated by the functional groups of this loop is incompatible with CMP or GMP binding, a result consistent with NMR titration experiments showing that binding affinities of UMP (0.12 mM) and AMP (0.26 mM) are 30-fold lower than those measured for either CMP (3.6 mM) or GMP (3.3 mM) (24). The MID domain also bears two invariant lysines that recognize the 5′-terminal phosphate present in silencing RNAs (6). A crystal structure of an *Archaeoglobus fulgidus* PIWI enzyme provided the first information on the conformation of a guide strand bound in a MID domain (71). The RNA is bound such that the 5′-terminal base is kinked and buried and unavailable for base-pairing, as observed in the guide-bound structure of human Ago2 (51) (**Figure 5*b***). This finding provides an explanation for previous biochemical observations that 5′-terminal base identity is unimportant in target recognition (51).

Target recognition, slicer activity, and conformational changes. A series of structures characterizing full-length archaeal Argonautes has provided crucial details on the protein's catalytic mechanism, its interaction with a guide strand to form a competent RISC, and the orientation of ternary complexes formed in the presence of the passenger strand or a target ssRNA. A crystal structure of Argonaute from *Pyrococcus furiosus* revealed that the PIWI domain adopts an RNase H–like fold, implicating it as the catalytic domain and site of slicer activity (83). Similar to the requirements for RNaseH activity, RISC-catalyzed RNA cleavage requires divalent metal ions and yields a 5′ product, which has a free 3′ hydroxyl group, and a 3′ product, which carries a 5′ phosphate group. Crystal structures of *Thermus thermophilus* Argonaute bound to a DNA approximating the guide strand and an RNA target show a PIWI domain bearing a catalytic triad of aspartic acid residues that coordinates a pair of magnesium ions at an appropriate distance from the target strand's cleavage site (94) (**Figure 5*f***). This catalytic triad DDX (where X is Asp or His) motif was initially identified in catalytically active Argonautes, is absent from those lacking slicer activity, and appears to contrast with the catalytic tetrad DEDD motif characteristic of RNase H enzymes (65). Curiously, the second magnesium ion could be observed only when crystallization conditions were adjusted from 50 to 80 mM Mg^{2+}.

Despite the B-form propensity of the DNA guide present in the *T. thermophilus* structures, the guide-target duplex adopts the A-form geometry typical of a dsRNA double helix; a dsRNA duplex bound by *A. fulgidus* PIWI also adopts the A-form architecture (70). When *T. thermophilus* Argonaute is bound to a 12-nt target, the 3′ terminus of the guide remains bound by the PAZ domain; in contrast, binding to a 15-nt or longer target induces release of the guide's end from the PAZ domain in order to accommodate the two strands' extension beyond a full turn (11 nt) of the A-form helix (94) (**Figure 5*e***). Concomitant slicing assays suggest that the 3′ terminus of the guide strand must be released from the PAZ domain for cleavage to take place, which is consistent with the structural observations: Duplexes longer than a single turn can be oriented correctly for target strand cleavage only if the 3′ terminus of the guide strand is released. This finding supports the previously proposed two-state model and refutes the fixed-end model that anticipated both termini of the guide strand remaining anchored during all stages of target recognition (94). Functional

dispensability of 3′ terminus binding is further shown by mutations of the PAZ domain that have little effect on slicing assays, which contrasts with the loss of cleavage observed upon mutation of MID domain residues that recognize the 5′ terminus (95). Cleavage assays also demonstrate that bulges inserted into the guide's seed region prevent cleavage, whereas slicing can proceed in the presence of similar bulges in the same region of the target strand (93).

The conformation of the guide strand in the absence of target is of mechanistic significance. In crystal structures of guide-loaded Argonaute, the nucleic acid is bound in a central basic tract that spans the two lobes of the protein. The seed portion (positions 2–6) is typically well-ordered, while electron density has not been observed for nucleotides past position 10, with the exception of a PAZ-bound terminal nucleotide (19, 65, 77, 95). Recent eukaryotic Argonaute structures bearing a traditional guide strand of RNA reveal a preordered single helix in A-form geometry (19, 77) (**Figure 5*b***). The thermodynamic repercussions of an ordered guide strand were explored in a series of isothermal titration calorimetry experiments in the context of *A. fulgidus* PIWI (69).

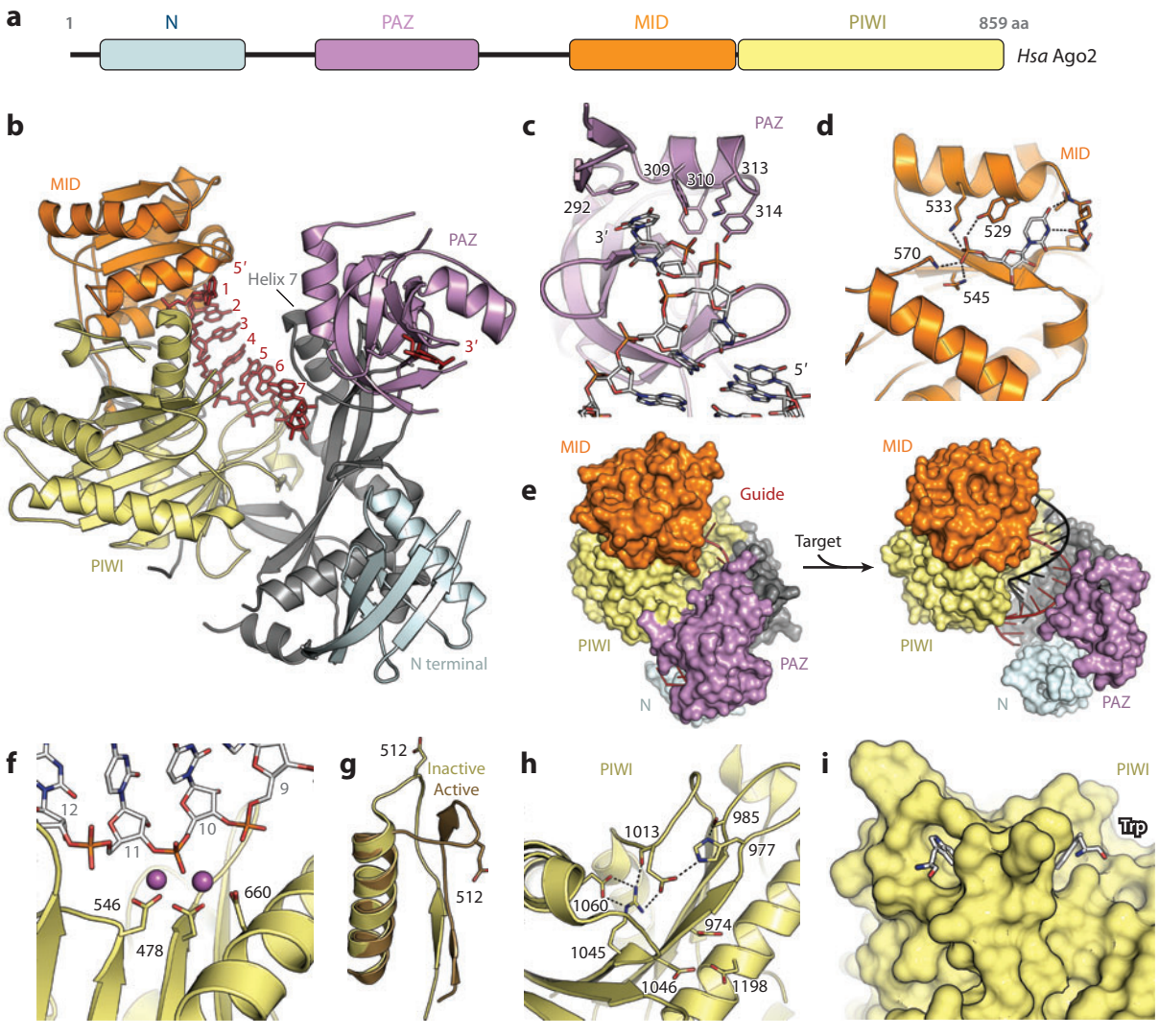

The study showed that a guide strand held in a helical conformation can increase the affinity for target up to ~300-fold by decreasing the entropic cost that would otherwise be associated with ordering of the guide. This essentially increases the effective melting temperature and the propensity for binding between guide and target, which is of particular importance in consideration of the prevalence of mismatches in the miRNA pathway.

Along with the reorientation of nucleic acid components upon RISC's binding of a target, the Argonaute protein has been observed or postulated to undergo its own rearrangements. A comparison of *T. thermophilus* Argonaute bound to a 10-nt versus a 21-nt guide shows moderate yet global reorientation of the protein (95). The 10-nt guide-bound conformation is likely similar to the unavailable free structure, and the observed motion is presumed to be necessary to accommodate a full-length guide strand. The two lobes shift conformation again when a target is bound to the *T. thermophilus* protein, widening to allow formation of a double helix in the tract that previously housed only the guide strand (93). Still another protein conformation is sampled when the guide-target duplex becomes long enough to induce 3′ terminus release from the PAZ domain as discussed above (**Figure 5*e***); this involves a pivoting of the PAZ domain and a substantial shift of the PIWI domain loops dubbed L1 and L2 (65, 94) (**Figure 5*g***). The significance of the L2 rearrangement became apparent upon determination of the structure of *K. polysporus* Argonaute, which bore a postrearrangement conformation with a glutamate residue of L2 positioned appropriately to act as a fourth catalytic residue in conjunction with the aforementioned three aspartic acids (65). This observation can be extended to reveal mechanistic details of the *T. thermophilus* enzyme: Upon sufficient base-pairing between guide and target to release the 3′ terminus from the PAZ domain, L2 shifts and deposits the final moiety of a catalytic tetrad, apparently acting as a trigger for catalysis (**Figure 5*h***). Thus, catalytically active Argonaute proteins indeed bear a DEDD (or DEDH in the case of human Ago2) catalytic tetrad as initially expected on the basis of the homology between the PIWI domain and RNase H enzymes, and

Figure 5

Snapshots of RISC in action. (*a*) The domain structure of Argonaute is relatively well conserved in the AGO clade. The PIWI clade proteins lack the N and PAZ domains. (*b*) The crystal structure of human Ago2 bound to an RNA guide strand (PDB ID: 4EI1). The seed region (nt 2–6) is prearranged in A-form geometry while the downstream portions of the guide strand cannot be modeled owing to disorder, as is typical in the absence of a target strand. Helix 7 is observed to rest against guide strand bases 6 and 7, distorting their geometry and providing an apparent barrier to target binding that is presumably circumvented via a conformational change. (*c*) The PAZ domain of human Ago2 recognizes the 3′-terminal 2-nt overhang typical of helices involved in RNAi (PDB ID: 1SI3). Conserved residues contacting the 3′ terminus are represented as sticks and are labeled. A hydrophobic pocket receives the terminal nucleobase. Nucleotides from the 5′ terminus can be seen at the bottom right, making only slight contact with the PAZ domain. (*d*) The MID domain is responsible for recognition of a phosphorylated 5′ terminus (PDB ID: 3LUJ). This UMP-bound crystal structure reveals the polar contacts that drive phosphate recognition as well as the base-specific contacts that grant the MID domain its preference for a 5′-terminal A or U. (*e*) A pair of *Thermus thermophilus* crystal structures illustrate a conformational change that results upon extensive base-pairing between guide and target strands (*left*, PDB ID: 3DLH; *right*, PDB ID: 3HM9). The RISC binding to a 19-nt target strand allows formation of an A-form helix that induces release of the guide strand's 3′ terminus from the PAZ domain along with a drastic opening of the two Argonaute lobes. The target-bound model shows that the N domain blocks formation of a longer helix. (*f*) In the catalytic center of *T. thermophilus* Argonaute's PIWI domain, three aspartic acid residues coordinate a pair of Mg^{2+} ions for cleavage of the target strand, shown as white sticks with nucleotides numbered in gray (PDB ID: 3HVR). (*g*) In *T. thermophilus* the target-induced conformation change also involves reorientation of L2, which contains a glutamic acid residue. If target binding is incomplete or absent, the inactive state (*yellow*) is sampled. In the target-bound state (*brown*), the glutamic acid is deposited adjacent to the aforementioned catalytic triad, completing a tetrad typical of RNase H enzymes (bound to a 12-nt target and inactive, PDB ID: 3HO1; bound to a 19-nt target and active, PDB ID: 3HM9). (*h*) The preordered catalytic tetrad observed in the absence of target strand in *Kluyveromyces polysporus* Argonaute (PDB ID: 4F1N). Residue 1013 here corresponds to *T. thermophilus* residue 512. (*i*) The PIWI domain of human Ago2 bears two tryptophan-binding sites that complement the side chain geometry expected from a GW protein binding partner (PDB ID: 4EI1). Free tryptophan was present in the crystallization conditions and the pair of bound amino acids is represented as sticks.

may undergo conformational change in response to target binding to facilitate selective catalytic activity (65).

The *K. polysporus* structure revealed an architecture allowing unobstructed formation of an extended guide-target duplex; this is in contrast to the *T. thermophilus* enzyme, where the N domain would sterically clash with any such duplex longer than 16 bp (65). The eukaryotic enzyme permits this by a rotation of the N domain. In the case of the human Ago2 structure, a potential steric clash is introduced: Helix 7 abuts and slightly reorients the seventh nucleobase of the guide strand, and its observed location would preclude target strand binding (77) (**Figure 5*b***). Helix 7 has been proposed to facilitate passenger strand release and/or to perform readout of miRNA target recognition that would be coupled to its necessary reorientation upon target binding (77).

Interactions between Argonaute and other proteins. The interaction between human Argonaute and Dicer can be revisited in light of recent structural progress. As discussed above, the 58-aa PIWI-box was previously identified as the minimal portion of Argonaute sufficient for Dicer binding (85). It is now apparent that the PIWI-box constitutes a three-stranded β-sheet from the middle of the PIWI domain. Interestingly, most of this subdomain is occluded in the context of the full protein, leaving few reasonable options for intermolecular contacts with Dicer. However, if a ∼10-aa stretch (bearing four proline residues) of Argonaute's N terminus were peeled away from the surface of the PIWI-box, it would reveal a much larger potential binding interface. Continued structural study is necessary to verify the nature of an interaction that is probably vital for RISC loading.

Three of the four human AGO proteins lack slicing activity, yet they remain capable of inducing robust translational repression. This is brought about by Argonaute recruiting glycine- and tryptophan-rich GW proteins that are components of the P body wherein mRNAs are degraded. One such protein, GW182, contains multiple binding sites for Ago2 (86). The crystal structure of human Ago2 was determined in the presence of free tryptophan, revealing two pockets that each bind a tryptophan molecule primarily via hydrophobic interactions (77) (**Figure 5*i***). Both the 24 Å spacing between pockets and the orientation of the carboxyl and amino groups of the bound amino acids are consistent with the geometry plausible for a pair of tryptophans in the context of a protein sequence with 8–14 aa between them, as is commonly found in GW proteins (77). This finding likely reveals the mechanism by which the PIWI domain of human Ago2 serves as an interaction platform for additional components of the RNAi machinery, as previously suspected (88).

GW-PABP Interface

The target-bound RISC binds GW proteins, which in turn form complexes localizing other cellular machinery to enact silencing. One such GW protein–induced recruitment is of poly(A)-binding proteins (PABPs). PABP binds the 3′ poly(A) tail of mRNA and recruits PAIP1 and eIF4G to promote translation initiation via mRNA circularization (21). The competing PABP interaction with a GW protein likely inverts these effects, inhibiting translation initiation and inducing deadenylation, followed by message degradation. The interaction between the GW protein TNRC6C and polyadenylate-binding protein 1 (PABPC1) has been characterized, revealing recognition of a disordered region of a DUF domain from TNRC6 by the α-helical C-terminal domain of PABPC1 (39) (**Figure 6*a***). The TNRC6C-interacting surface of PABPC1 overlaps with that used to bind PAIP1, suggesting the interactions are mutually exclusive. Concomitant assays in mammalian cell extracts demonstrated that mutations at the TNRC6C-PABPC1 interface impair mRNA deadenylation, providing evidence for this interaction's role in miRNA-mediated silencing (39).

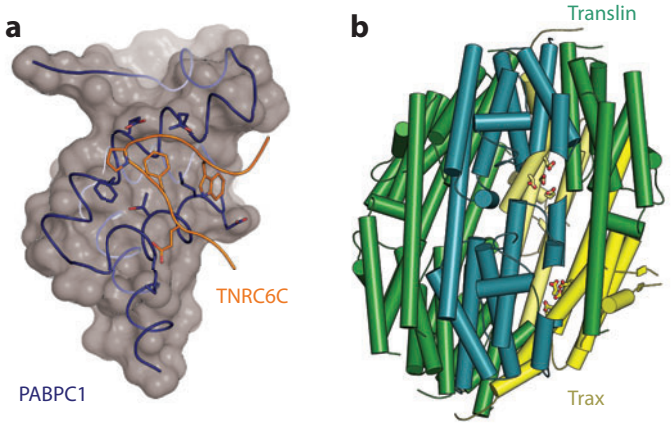

Figure 6

Molecular assemblies in RNAi. (*a*) The interface between the C-terminal portion of PABPC1 and the DUF domain of TNRC6C, a GW protein (PDB ID: 2X04). Interacting side chains are shown as sticks. (*b*) The human endonuclease C3PO comprises hetero- and homodimers of Trax (*yellow*) and/or Translin (*green and teal*). The teal-colored Translin homodimer in the foreground is partially cut away to reveal the side chains of Trax's active site, rendered as sticks. In this crystal structure, the complex adopts a hollow, egg-like shape with no obvious means for its passenger strand substrate to access the enclosed active sites (PDB ID: 3PJA).

C3PO

Once pre-RISC has been assembled, Argonaute's slicing activity can promote passenger strand dissociation. This dissociation and subsequent RISC activation are inhibited when slicing is inhibited either by Argonaute mutations, via protecting modifications to the passenger strand, or by Argonautes that lack catalytic activity (62, 63). RISC activation is promoted by the exonuclease C3PO, which binds, nicks, and subsequently degrades the passenger strand of pre-RISC (100). C3PO comprises a multimeric assembly of Trax and Translin protomers. Each protomer adopts the same fold, but only Trax bears endonuclease activity. Recent crystal structures contain assemblies of Trax:Translin protomers in a ratio of 2:6 or 2:4 depending on the use of full-length or slightly truncated constructs (87, 100) (**Figure 6*b***). Curiously, the observed C3PO complexes form hollow egg-shaped enclosures, with an inner surface that bears the residues responsible for catalysis as well as an extensive positively charged surface that likely binds ssRNA (87, 100). This architecture poses a mystery: How does the passenger strand substrate reach the inaccessible Trax active sites? It has been proposed that the substrate encounters the catalytic core either via a gap-generating conformational change of the multimeric complex, or by a partial dissociation of the assembly. Observations from native mass spectrometry of the C3PO complex support the latter possibility; diverse assemblies were detected, including Trax:Translin ratios of 6:1, 6:2, 5:2, 5:3, and 4:3 (87).

FRONTIERS IN RNAi BIOPHYSICS

Strand Selection

Some of the most recalcitrant questions regarding RNAi pertain to the mechanisms of strand selection. Although the sequence-level tendencies are well documented, it remains unclear how guide and passenger strands are distinguished at the molecular level (33). Argonaute's MID domain

binds the 5′-terminal nucleobase selectively, generating a strong preference that varies depending on the Argonaute and can be detected empirically by deep sequencing of small RNAs (33, 41). In addition, the RNAi duplex bearing the 5′ terminus and participating in less thermodynamically stable base-pairing is more likely to be loaded as the guide strand. The orientation of dicing does not determine guide strand identity (67, 73), and it has been reported that an RNAi dsRBP can act as an asymmetry sensor (18, 89) and/or as a functional bridge between Dicer and Argonaute (10). Interestingly, it has been difficult to assign the precise mechanisms responsible for the detection of thermodynamic asymmetry, probably because it is a dynamic process involving nuanced action by multiple proteins.

P Bodies

P bodies are cytoplasmic foci of RNA-driven silencing (reviewed in Reference 44) and are home to a host of proteins that cooperate to degrade an mRNA that has been targeted by RISC. These regions are defined by a sprawling network of protein-protein interactions, with a structural glimpse provided by recent insight into the interfaces between GW proteins and PABPs or Argonaute proteins (39, 77). Because the structures of many individual RNAi pathway proteins are now known, future structural biology efforts must focus on the binding sites between the players and the mechanisms by which they colocalize.

Kinetics of Repression, Decay, and RISC Turnover

An mRNA targeted by a nonslicing RISC is subject to translational repression, deadenylation, and exonucleolytic degradation, but the timing, mechanistic coupling, and relative importance of these processes have not been determined (reviewed in Reference 15). In the wake of cell-based studies implicating mRNA decay as the primary mode of silencing based on 12- and 32-h time points (30), two similar studies, each using multiple 2-h time points, demonstrated for the first time that translational repression precedes deadenylation and decay of a targeted miRNA (1, 16). These studies revealed the importance of kinetics in the silencing pathway. Impending studies will be especially illuminating if they are able to improve on the 2-h resolution used in recent experiments and/or track single molecules instead of population kinetics.

Another unresolved kinetic question pertains to the lifetime of the RISC complex. While RISC-protected small RNAs were initially thought to have half-lives on the order of days, recent reports have shown these RNAs to be substrates for degradation by enzymes such as XRN2 (reviewed in Reference 28). The lifetime (and determinants thereof) of a given intact RISC will have profound repercussions on understanding miRNA function and successful design of siRNA-based therapies, so this area of inquest is fertile ground for biophysical study.

SUMMARY POINTS

1. The central macromolecules and interactions of the RNAi pathway have been identified, with increasing mechanistic insight provided by structural models.
2. A wealth of Argonaute structures has revealed the protein-RNA interactions central to RNAi.
3. The molecular architecture of Dicer is known, elucidating how different Dicers produce products of varying lengths.

FUTURE ISSUES

1. What is the architecture of the microprocessor complex and how does it facilitate recognition of the stem-ssRNA junction?
2. Human Dicer lacks a high-resolution structure, and there are no RNA-bound Dicer structures available for any organism.
3. How does the RISC-loading complex perform the subtle task of strand selection?
4. What are the structural details of key protein-protein interfaces such as Argonaute–GW protein, Argonaute-Dicer, Dicer-dsRBP, and Drosha-DGCR8?
5. What are the spatial and kinetic properties of silencing processes downstream of RISC assembly?

DISCLOSURE STATEMENT

The authors are not aware of any affiliations, memberships, funding, or financial holdings that might be perceived as affecting the objectivity of this review.

ACKNOWLEDGMENTS

This work is dedicated to Carolen Koleszar, former mentor to R.W. The authors are grateful to Mary Anne Kidwell, Ho Young Lee, and Cameron Noland for critical comments on the manuscript. We appreciate the contributions to **Figure 3** made by Pick-Wei Lau and Ian MacRae. We thank Mark Glover and Stephen Chaulk for helpful communication. Support from the NIH to R.W. is gratefully acknowledged (F32GM096689). J.D. is an investigator of the Howard Hughes Medical Institute.

LITERATURE CITED

1. Bazzini AA, Lee MT, Giraldez AJ. 2012. Ribosome profiling shows that miR-430 reduces translation before causing mRNA decay in zebrafish. *Science* 336(6078):233–37
2. Bellemer C, Bortolin-Cavaillé M-L, Schmidt U, Jensen SMR, Kjems J, et al. 2012. Microprocessor dynamics and interactions at endogenous imprinted C19MC microRNA genes. *J. Cell. Sci.* 125(Pt. 11):2709–20
3. Berezikov E. 2011. Evolution of microRNA diversity and regulation in animals. *Nat. Rev. Genet.* 12(12):846–60
4. Bernstein E, Caudy AA, Hammond SM, Hannon GJ. 2001. Role for a bidentate ribonuclease in the initiation step of RNA interference. *Nature* 409(6818):363–66
5. Boland A, Huntzinger E, Schmidt S, Izaurralde E, Weichenrieder O. 2011. Crystal structure of the MID-PIWI lobe of a eukaryotic Argonaute protein. *Proc. Natl. Acad. Sci. USA* 108(26):10466–71
6. Boland A, Tritschler F, Heimstädt S, Izaurralde E, Weichenrieder O. 2010. Crystal structure and ligand binding of the MID domain of a eukaryotic Argonaute protein. *EMBO Rep.* 11(7):522–27
7. Carthew RW, Sontheimer EJ. 2009. Origins and mechanisms of miRNAs and siRNAs. *Cell* 136(4):642–55
8. Castanotto D, Sakurai K, Lingeman R, Li H, Shively L, et al. 2007. Combinatorial delivery of small interfering RNAs reduces RNAi efficacy by selective incorporation into RISC. *Nucleic Acids Res.* 35(15):5154–64
9. Cenik ES, Fukunaga R, Lu G, Dutcher R, Wang Y, et al. 2011. Phosphate and R2D2 restrict the substrate specificity of Dicer-2, an ATP-driven ribonuclease. *Mol. Cell* 42:172–84

10. Chendrimada TP, Gregory RI, Kumaraswamy E, Norman J, Cooch N, et al. 2005. TRBP recruits the Dicer complex to Ago2 for microRNA processing and gene silencing. *Nature* 436(7051):740–44
11. Chiu Y-L, Rana TM. 2003. siRNA function in RNAi: a chemical modification analysis. *RNA* 9(9):1034–48
12. Curtin SJ, Watson JM, Smith NA, Eamens AL, Blanchard CL, Waterhouse PM. 2008. The roles of plant dsRNA-binding proteins in RNAi-like pathways. *FEBS Lett.* 582(18):2753–60
13. Daniels SM, Melendez-Peña CE, Scarborough RJ, Daher A, Christensen HS, et al. 2009. Characterization of the TRBP domain required for Dicer interaction and function in RNA interference. *BMC Mol. Biol.* 10(1):38
14. Davidson BL, McCray PB. 2011. Current prospects for RNA interference-based therapies. *Nat. Rev. Genet.* 12(5):329–40
15. Djuranovic S, Nahvi A, Green R. 2011. A parsimonious model for gene regulation by miRNAs. *Science* 331(6017):550–53
16. Djuranovic S, Nahvi A, Green R. 2012. miRNA-mediated gene silencing by translational repression followed by mRNA deadenylation and decay. *Science* 336(6078):237–40
17. Doyle M, Jantsch MF. 2002. New and old roles of the double-stranded RNA-binding domain. *J. Struct. Biol.* 140(1–3):147–53
18. Eamens AL, Smith NA, Curtin SJ, Wang M-B, Waterhouse PM. 2009. The *Arabidopsis thaliana* double-stranded RNA binding protein DRB1 directs guide strand selection from microRNA duplexes. *RNA* 15(12):2219–35
19. Elkayam E, Kuhn C-D, Tocilj A, Haase AD, Greene EM, et al. 2012. The structure of human Argonaute-2 in complex with miR-20a. *Cell* 150:100–10
20. Eulalio A, Huntzinger E, Izaurralde E. 2008. GW182 interaction with Argonaute is essential for miRNA-mediated translational repression and mRNA decay. *Nat. Struct. Mol. Biol.* 15(4):346–53
21. Fabian MR, Sonenberg N. 2012. The mechanics of miRNA-mediated gene silencing: a look under the hood of miRISC. *Nat. Struct. Mol. Biol.* 19(6):586–93
22. Fabian MR, Sonenberg N, Filipowicz W. 2010. Regulation of mRNA translation and stability by microRNAs. *Annu. Rev. Biochem.* 79:351–79
23. Faller M, Toso D, Matsunaga M, Atanasov I, Senturia R, et al. 2010. DGCR8 recognizes primary transcripts of microRNAs through highly cooperative binding and formation of higher-order structures. *RNA* 16(8):1570–83
24. Frank F, Sonenberg N, Nagar B. 2010. Structural basis for 5′-nucleotide base-specific recognition of guide RNA by human AGO2. *Nature* 465(7299):818–22
25. Fukunaga R, Han BW, Hung J-H, Xu J, Weng Z, Zamore PD. 2012. Dicer partner proteins tune the length of mature miRNAs in flies and mammals. *Cell* 151(3):533–46
26. Gan J, Tropea JE, Austin BP, Court DL, Waugh DS, Ji X. 2006. Structural insight into the mechanism of double-stranded RNA processing by ribonuclease III. *Cell* 124(2):355–66
27. Gregory RI, Yan K-P, Amuthan G, Chendrimada T, Doratotaj B, et al. 2004. The microprocessor complex mediates the genesis of microRNAs. *Nature* 432(7014):235–40
28. Großhans H, Chatterjee S. 2011. MicroRNases and the regulated degradation of mature animal miRNAs. *Adv. Exp. Mol. Biol.* 700:140–55
29. Gunawardane LS, Saito K, Nishida KM, Miyoshi K, Kawamura Y, et al. 2007. A slicer-mediated mechanism for repeat-associated siRNA 5′ end formation in *Drosophila*. *Science* 315(5818):1587–90
30. Guo H, Ingolia NT, Weissman JS, Bartel DP. 2010. Mammalian microRNAs predominantly act to decrease target mRNA levels. *Nature* 466(7308):835–40
31. Han J, Lee Y, Yeom K-H, Nam J-W, Heo I, et al. 2006. Molecular basis for the recognition of primary microRNAs by the Drosha-DGCR8 complex. *Cell* 125(5):887–901
32. Hartig JV, Förstemann K. 2011. Loqs-PD and R2D2 define independent pathways for RISC generation in *Drosophila*. *Nucleic Acids Res.* 39(9):3836–51
33. Hu H, Yan Z, Xu Y, Hu H, Menzel C, et al. 2009. Sequence features associated with microRNA strand selection in humans and flies. *BMC Genomics* 10(1):413
34. Huang Y, Ji L, Huang Q, Vassylyev DG, Chen X, Ma J-B. 2009. Structural insights into mechanisms of the small RNA methyltransferase HEN1. *Nature* 461(7265):823–27

35. Ipsaro JJ, Haase AD, Knott SR, Joshua-Tor L, Hannon GJ. 2012. The structural biochemistry of Zucchini implicates it as a nuclease in piRNA biogenesis. *Nature* 491(7423):279–83
36. Jackson RJ, Standart N. 2007. How do microRNAs regulate gene expression? *Sci. STKE* 2007(367):re1
37. Janowski BA, Huffman KE, Schwartz JC, Ram R, Nordsell R, et al. 2006. Involvement of AGO1 and AGO2 in mammalian transcriptional silencing. *Nat. Struct. Mol. Biol.* 13(9):787–92
38. Jinek M, Doudna JA. 2009. A three-dimensional view of the molecular machinery of RNA interference. *Nature* 457(7228):405–12
39. Jinek M, Fabian MR, Coyle SM, Sonenberg N, Doudna JA. 2010. Structural insights into the human GW182-PABC interaction in microRNA-mediated deadenylation. *Nat. Struct. Mol. Biol.* 17(2):238–40
40. Kataoka N, Fujita M, Ohno M. 2009. Functional association of the microprocessor complex with the spliceosome. *Mol. Cell. Biol.* 29(12):3243–54
41. Kawamata T, Tomari Y. 2010. Making RISC. *Trends Biochem. Sci.* 35(7):368–76
42. Kim Y-K, Kim VN. 2007. Processing of intronic microRNAs. *EMBO J.* 26(3):775–83
43. Kowalinski E, Lunardi T, McCarthy AA, Louber J, Brunel J, et al. 2011. Structural basis for the activation of innate immune pattern-recognition receptor RIG-I by viral RNA. *Cell* 147(2):423–35
44. Kulkarni M, Ozgur S, Stoecklin G. 2010. On track with P-bodies. *Biochem. Soc. Trans.* 38(1):242
45. Laraki G, Clerzius G, Daher A, Melendez-Peña C, Daniels S, Gatignol A. 2008. Interactions between the double-stranded RNA-binding proteins TRBP and PACT define the Medipal domain that mediates protein-protein interactions. *RNA Biol.* 5(2):92–103
46. Lau P-W, Guiley KZ, De N, Potter CS, Carragher B, MacRae IJ. 2012. The molecular architecture of human Dicer. *Nat. Struct. Mol. Biol.* 19(4):436–40
47. Lee HY, Doudna JA. 2012. TRBP alters human precursor microRNA processing in vitro. *RNA* 18(11):2012–19
48. Lee RC, Feinbaum RL, Ambros V. 1993. The *C. elegans* heterochronic gene *lin-4* encodes small RNAs with antisense complementarity to *lin-14*. *Cell* 75(5):843–54
49. Lee Y, Ahn C, Han J, Choi H, Kim J, et al. 2003. The nuclear RNase III Drosha initiates microRNA processing. *Nature* 425(6956):415–19
50. Lee Y, Hur I, Park S-Y, Kim Y-K, Suh MR, Kim VN. 2006. The role of PACT in the RNA silencing pathway. *EMBO J.* 25(3):522–32
51. Lewis BP, Burge CB, Bartel DP. 2005. Conserved seed pairing, often flanked by adenosines, indicates that thousands of human genes are microRNA targets. *Cell* 120(1):15–20
52. Lingel A, Simon B, Izaurralde E, Sattler M. 2004. Nucleic acid 3′-end recognition by the Argonaute2 PAZ domain. *Nat. Struct. Mol. Biol.* 11(6):576–77
53. Lu M, Zhang Q, Deng M, Miao J, Guo Y, et al. 2008. An analysis of human microRNA and disease associations. *PLoS ONE* 3(10):e3420
54. Lund E, Dahlberg JE. 2006. Substrate selectivity of exportin 5 and Dicer in the biogenesis of microRNAs. *Cold Spring Harb. Symp. Quant. Biol.* 71:59–66
55. Ma E, MacRae IJ, Kirsch JF, Doudna JA. 2008. Autoinhibition of human Dicer by its internal helicase domain. *J. Mol. Biol.* 380(1):237–43
56. Ma E, Zhou K, Kidwell MA, Doudna JA. 2012. Coordinated activities of human Dicer domains in regulatory RNA processing. *J. Mol. Biol.* 422:466–76
57. Ma J-B, Ye K, Patel DJ. 2004. Structural basis for overhang-specific small interfering RNA recognition by the PAZ domain. *Nature* 429(6989):318–22
58. MacFarlane L-A, Murphy PR. 2010. MicroRNA: biogenesis, function and role in cancer. *Curr. Genomics* 11(7):537–61
59. MacRae IJ. 2006. Structural basis for double-stranded RNA processing by Dicer. *Science* 311(5758):195–98
60. MacRae IJ, Doudna JA. 2007. Ribonuclease revisited: structural insights into ribonuclease III family enzymes. *Curr. Opin. Struct. Biol.* 17(1):138–45
61. MacRae IJ, Ma E, Zhou M, Robinson CV, Doudna JA. 2008. In vitro reconstitution of the human RISC-loading complex. *Proc. Natl. Acad. Sci. USA* 105(2):512–17
62. Maiti M, Lee H-C, Liu Y. 2007. QIP, a putative exonuclease, interacts with the *Neurospora* Argonaute protein and facilitates conversion of duplex siRNA into single strands. *Genes Dev.* 21(5):590–600

63. Matranga C, Tomari Y, Shin C, Bartel DP, Zamore PD. 2005. Passenger-strand cleavage facilitates assembly of siRNA into Ago2-containing RNAi enzyme complexes. *Cell* 123(4):607–20
64. Mueller GA, Miller MT, Derose EF, Ghosh M, London RE, Hall TMT. 2010. Solution structure of the Drosha double-stranded RNA-binding domain. *Silence* 1(1):2
65. Nakanishi K, Weinberg DE, Bartel DP, Patel DJ. 2012. Structure of yeast Argonaute with guide RNA. *Nature* 486:368–74
66. Nishimasu H, Ishizu H, Saito K, Fukuhara S, Kamatani MK, et al. 2012. Structure and function of Zucchini endoribonuclease in piRNA biogenesis. *Nature* 491(7423):284–87
67. Noland CL, Ma E, Doudna JA. 2011. siRNA repositioning for guide strand selection by human Dicer complexes. *Mol. Cell* 43(1):110–21
68. Okamura K, Robine N, Liu Y, Liu Q, Lai EC. 2011. R2D2 organizes small regulatory RNA pathways in *Drosophila*. *Mol. Cell. Biol.* 31(4):884–96
69. Parker JS, Parizotto EA, Wang M, Roe SM, Barford D. 2009. Enhancement of the seed-target recognition step in RNA silencing by a PIWI/MID domain protein. *Mol. Cell* 33(2):204–14
70. Parker JS, Roe SM, Barford D. 2004. Crystal structure of a PIWI protein suggests mechanisms for siRNA recognition and slicer activity. *EMBO J.* 23(24):4727–37
71. Parker JS, Roe SM, Barford D. 2005. Structural insights into mRNA recognition from a PIWI domain-siRNA guide complex. *Nature* 434(7033):663–66
72. Paroo Z, Ye X, Chen S, Liu Q. 2009. Phosphorylation of the human microRNA-generating complex mediates MAPK/Erk signaling. *Cell* 139(1):112–22
73. Preall JB, He Z, Gorra JM, Sontheimer EJ. 2006. Short interfering RNA strand selection is independent of dsRNA processing polarity during RNAi in *Drosophila*. *Curr. Biol.* 16(5):530–35
74. Qin H, Chen F, Huan X, Machida S, Song J, Yuan YA. 2010. Structure of the *Arabidopsis thaliana* DCL4 DUF283 domain reveals a noncanonical double-stranded RNA-binding fold for protein-protein interaction. *RNA* 16(3):474–81
75. Saini HK, Griffiths-Jones S, Enright AJ. 2007. Genomic analysis of human microRNA transcripts. *Proc. Natl. Acad. Sci. USA* 104(45):17719–24
76. Sasaki T, Shimizu N. 2007. Evolutionary conservation of a unique amino acid sequence in human DICER protein essential for binding to Argonaute family proteins. *Gene* 396(2):312–20
77. Schirle NT, MacRae IJ. 2012. The crystal structure of human Argonaute2. *Science* 336(6084):1037–40
78. Schwarz DS, Hutvágner G, Du T, Xu Z, Aronin N, Zamore PD. 2003. Asymmetry in the assembly of the RNAi enzyme complex. *Cell* 115(2):199–208
79. Senturia R, Faller M, Yin S, Loo JA, Cascio D, et al. 2010. Structure of the dimerization domain of DiGeorge critical region 8. *Protein Sci.* 19(7):1354–65
80. Shabalina SA, Koonin EV. 2008. Origins and evolution of eukaryotic RNA interference. *Trends Ecol. Evol.* 23(10):578–87
81. Sohn SY, Bae WJ, Kim JJ, Yeom K-H, Kim VN, Cho Y. 2007. Crystal structure of human DGCR8 core. *Nat. Struct. Mol. Biol.* 14(9):847–53
82. Soifer HS, Sano M, Sakurai K, Chomchan P, Saetrom P, et al. 2008. A role for the Dicer helicase domain in the processing of thermodynamically unstable hairpin RNAs. *Nucleic Acids Res.* 36(20):6511–22
83. Song J-J, Smith SK, Hannon GJ, Joshua-Tor L. 2004. Crystal structure of Argonaute and its implications for RISC slicer activity. *Science* 305(5689):1434–37
84. Sun W, Pertzev A, Nicholson AW. 2005. Catalytic mechanism of *Escherichia coli* ribonuclease III: kinetic and inhibitor evidence for the involvement of two magnesium ions in RNA phosphodiester hydrolysis. *Nucleic Acids Res.* 33(3):807–15
85. Tahbaz N, Kolb FA, Zhang H, Jaronczyk K, Filipowicz W, Hobman TC. 2004. Characterization of the interactions between mammalian PAZ PIWI domain proteins and Dicer. *EMBO Rep.* 5(2):189–94
86. Takimoto K, Wakiyama M, Yokoyama S. 2009. Mammalian GW182 contains multiple Argonaute-binding sites and functions in microRNA-mediated translational repression. *RNA* 15(6):1078–89
87. Tian Y, Simanshu DK, Ascano M, Diaz-Avalos R, Park AY, et al. 2011. Multimeric assembly and biochemical characterization of the Trax-translin endonuclease complex. *Nat. Struct. Mol. Biol.* 18(6):658–64

88. Till S, Lejeune E, Thermann R, Bortfeld M, Hothorn M, et al. 2007. A conserved motif in Argonaute-interacting proteins mediates functional interactions through the Argonaute PIWI domain. *Nat. Struct. Mol. Biol.* 14(10):897–903
89. Tomari Y. 2004. A protein sensor for siRNA asymmetry. *Science* 306(5700):1377–80
90. Tsutsumi A, Kawamata T, Izumi N, Seitz H, Tomari Y. 2011. Recognition of the pre-miRNA structure by *Drosophila* Dicer-1. *Nat. Struct. Mol. Biol.* 18(10):1153–58
91. Voigt F, Reuter M, Kasaruho A, Schulz EC, Pillai RS, Barabas O. 2012. Crystal structure of the primary piRNA biogenesis factor Zucchini reveals similarity to the bacterial PLD endonuclease Nuc. *RNA* 18(12):2128–34
92. Wang H-W, Noland C, Siridechadilok B, Taylor DW, Ma E, et al. 2009. Structural insights into RNA processing by the human RISC-loading complex. *Nat. Struct. Mol. Biol.* 16(11):1148–53
93. Wang Y, Juranek S, Li H, Sheng G, Tuschl T, Patel DJ. 2008. Structure of an Argonaute silencing complex with a seed-containing guide DNA and target RNA duplex. *Nature* 456(7224):921–26
94. Wang Y, Juranek S, Li H, Sheng G, Wardle GS, et al. 2009. Nucleation, propagation and cleavage of target RNAs in Ago silencing complexes. *Nature* 461(7265):754–61
95. Wang Y, Sheng G, Juranek S, Tuschl T, Patel DJ. 2008. Structure of the guide-strand-containing argonaute silencing complex. *Nature* 456(7219):209–13
96. Weinberg DE, Nakanishi K, Patel DJ, Bartel DP. 2011. The inside-out mechanism of Dicers from budding yeasts. *Cell* 146(2):262–76
97. Welker NC, Maity TS, Ye X, Aruscavage PJ, Krauchuk AA, et al. 2011. Dicer's helicase domain discriminates dsRNA termini to promote an altered reaction mode. *Mol. Cell* 41(5):589–99
98. Yamashita S, Nagata T, Kawazoe M, Takemoto C, Kigawa T, et al. 2010. Structures of the first and second double-stranded RNA-binding domains of human TAR RNA-binding protein. *Protein Sci.* 20(1):118–30
99. Yan KS, Yan S, Farooq A, Han A, Zeng L, Zhou M-M. 2003. Structure and conserved RNA binding of the PAZ domain. *Nature* 426(6965):468–74
100. Ye X, Huang N, Liu Y, Paroo Z, Huerta C, et al. 2011. Structure of C3PO and mechanism of human RISC activation. *Nat. Struct. Mol. Biol.* 18(6):650–57
101. Zeng Y, Cullen BR. 2005. Efficient processing of primary microRNA hairpins by Drosha requires flanking nonstructured RNA sequences. *J. Biol. Chem.* 280(30):27595–603
102. Zeng Y, Yi R, Cullen BR. 2005. Recognition and cleavage of primary microRNA precursors by the nuclear processing enzyme Drosha. *EMBO J.* 24(1):138–48
103. Zhang H, Kolb FA, Brondani V, Billy E, Filipowicz W. 2002. Human Dicer preferentially cleaves dsRNAs at their termini without a requirement for ATP. *EMBO J.* 21(21):5875–85
104. Zou J, Chang M, Nie P, Secombes CJ. 2009. Origin and evolution of the RIG-I like RNA helicase gene family. *BMC Evol. Biol.* 9:85

Annual Review of Biophysics
Volume 42, 2013

Contents

Doing Molecular Biophysics: Finding, Naming, and Picturing Signal Within Complexity
Jane S. Richardson and David C. Richardson 1

Structural Biology of the Proteasome
Erik Kish-Trier and Christopher P. Hill 29

Common Folds and Transport Mechanisms of Secondary Active Transporters
Yigong Shi 51

Coarse-Graining Methods for Computational Biology
Marissa G. Saunders and Gregory A. Voth 73

Electrophysiological Characterization of Membrane Transport Proteins
Christof Grewer, Armanda Gameiro, Thomas Mager, and Klaus Fendler 95

Entropy-Enthalpy Compensation: Role and Ramifications in Biomolecular Ligand Recognition and Design
John D. Chodera and David L. Mobley 121

Molecular Mechanisms of Drug Action: An Emerging View
James M. Sonner and Robert S. Cantor 143

The Underappreciated Role of Allostery in the Cellular Network
Ruth Nussinov, Chung-Jung Tsai, and Buyong Ma 169

Structural Insights into the Evolution of the Adaptive Immune System
Lu Deng, Ming Luo, Alejandro Velikovsky, and Roy A. Mariuzza 191

Molecular Mechanisms of RNA Interference
Ross C. Wilson and Jennifer A. Doudna 217

Molecular Traffic Jams on DNA
Ilya J. Finkelstein and Eric C. Greene 241

Advances, Interactions, and Future Developments in the CNS, Phenix, and Rosetta Structural Biology Software Systems
Paul D. Adams, David Baker, Axel T. Brunger, Rhiju Das, Frank DiMaio, Randy J. Read, David C. Richardson, Jane S. Richardson, and Thomas C. Terwilliger 265

Considering Protonation as a Posttranslational Modification Regulating Protein Structure and Function
André Schönichen, Bradley A. Webb, Matthew P. Jacobson, and Diane L. Barber 289

Energy Functions in De Novo Protein Design: Current Challenges and Future Prospects
Zhixiu Li, Yuedong Yang, Jian Zhan, Liang Dai, and Yaoqi Zhou 315

Quantitative Modeling of Bacterial Chemotaxis: Signal Amplification and Accurate Adaptation
Yuhai Tu 337

Influences of Membrane Mimetic Environments on Membrane Protein Structures
Huan-Xiang Zhou and Timothy A. Cross 361

High-Speed AFM and Applications to Biomolecular Systems
Toshio Ando, Takayuki Uchihashi, and Noriyuki Kodera 393

Super-Resolution in Solution X-Ray Scattering and Its Applications to Structural Systems Biology
Robert P. Rambo and John A. Tainer 415

Molecular Basis of NF-κB Signaling
Johanna Napetschnig and Hao Wu 443

Regulation of Noise in Gene Expression
Alvaro Sanchez, Sandeep Choubey, and Jane Kondev 469

Evolution in Microbes
Edo Kussell 493

Protein Structure Determination by Magic-Angle Spinning Solid-State NMR, and Insights into the Formation, Structure, and Stability of Amyloid Fibrils
Gemma Comellas and Chad M. Rienstra 515

Structural Studies of RNase P
Alfonso Mondragón 537

On the Universe of Protein Folds
Rachel Kolodny, Leonid Pereyaslavets, Abraham O. Samson, and Michael Levitt 559

Torque Measurement at the Single-Molecule Level
Scott Forth, Maxim Y. Sheinin, James Inman, and Michelle D. Wang 583

Modeling Gene Expression in Time and Space
Pau Rué and Jordi Garcia-Ojalvo 605

Mechanics of Dynamin-Mediated Membrane Fission
Sandrine Morlot and Aurélien Roux 629

Nanoconfinement and the Strength of Biopolymers
Tristan Giesa and Markus J. Buehler 651

Solid-State NMR of Nanomachines Involved in Photosynthetic Energy Conversion
A. Alia, Francesco Buda, Huub J.M. de Groot, and Jörg Matysik 675

Index

Cumulative Index of Contributing Authors, Volumes 38–42 701

Errata

An online log of corrections to *Annual Review of Biophysics* articles may be found at http://biophys.annualreviews.org/errata.shtml